Global J. Environ. Sci. Manage. 5(3): 319-330, Summer 2019

Global Journal of Environmental Science and Management
(GJESM)

Homepage: https://www.gjesm.net/

ORIGINAL RESEARCH PAPER

Remote sensing for urban heat and cool islands evaluation in semi-arid areas

M. Reisi[1,*], M. Ahmadi Nadoushan[2], L. Aye[3]

[1]*Department of Environmental Sciences, Faculty of Natural Resources, University of Kurdistan, Sanandaj, Iran*

[2]*Department of Environmental Sciences, Isfahan (Khorasgan) Branch, Islamic Azad University, Isfahan, Iran*

[3]*Renewable Energy and Energy Efficiency Group, Department of Infrastructure Engineering, Melbourne School of Engineering, The University of Melbourne, VIC 3010, Australia*

ARTICLE INFO

Article History:
Received 22 December 2018
Revised 29 March 2019
Accepted 09 May 2019

Keywords:
Landsat Land Surface Temperature (LST)
Land-Use/Land-Cover (LULC)
Urban Cool Island (UCIs)
Urban Heat Island (UHIs)
Semi-Arid Areas

ABSTRACT

Cities are experiencing rapid population growth and consequently extensive urbanization. Land-use/land-cover change is one of the important elements worldwide, which significantly affect the environment. This study aims to describe the emergence of urban heat and cool islands as a result of changes in land-use/land-cover. Land surface temperature over a 32-year period in Isfahan city, Iran was retrieved. The results confirmed the effect of land-use/land-cover change on Landsat land surface temperature. The average land surface temperature changed from 37.5°C in 1985 to 42.7°C in 2017 during August. The highest land surface temperature in the study area for both years occurred on bare soils (40.66°C in 1985 and 45.88°C in 2017). The second highest Landsat land surface temperature was recorded in central parts of the city with dense built-up covers (36.93°C in 1985 vs 42.45°C in 2017). The central parts of the city were found to have a lower Landsat land surface temperature compared to bare soils, which contributes to the formation of urban cool islands. As expected, water bodies and vegetation had a lower Landsat land surface temperature compared to other land covers. The results also showed changes in land use types during 1985 and 2017, with an increase in water bodies (148.82%) and built-up areas (39.67%) and a decrease in vegetation (20.08%) and bare soil (12.42%). The areas converted from vegetation to built-up experienced an increase in Landsat land surface temperature, which confirmed the effect of land-use/land-cover on microclimate.

DOI: 10.22034/gjesm.2019.03.05
©2019 GJESM. All rights reserved.

NUMBER OF REFERENCES	NUMBER OF FIGURES	NUMBER OF TABLES
56	5	4

*Corresponding Author:
Email: *m.reisi@uok.ac.ir*
Phone: +988733664600
Fax: +98733620550

Note: Discussion period for this manuscript open until October 1, 2019 on GJESM website at the "Show Article.

INTRODUCTION

Climate change started from pre-industrial ages and still continues (Orhan and Yakar, 2016). Intergovernmental Panel on Climate Change (IPCC) projected 1.4°C to 5.8°C increase in surface temperature by 2100 (Singh *et al.*, 2017). Climate change is a consequence of numerous natural and anthropogenic activities including deforestation, land use/cover (LULC) changes, and urbanization (Yıldırım *et al.*, 2011). Urbanization is posed as one of the most dominant anthropogenic phenomena, affecting the world since the 20th century (Singh *et al.*, 2017). Urbanization has reshaped the landscape significantly through LULC change (Jeevalakshmi *et al.*, 2017). Moreover, the Earth's vegetation cover has been decreasing as a result of urbanization, increasing more carbon dioxide accumulation in the atmosphere, that in turn changes surface energy circulation and local climate (Islam and Islam, 2013; Sun *et al.*, 2010). Higher temperature in urban areas compared to other land covers is referred to urban heat island (UHI) (Chen *et al.*, 2014; Amanollahi *et al.*, 2016). The UHI phenomenon was first defined by Luke Howard in early 1800s and ever since received extensive attentions due to its increasing effects (Howard, 1818). Urban heat islands (UHIs) are formed as a result of three phenomena. The main one is transformation of natural vegetated areas to non-evaporating and impervious surfaces (e.g. asphalt and tile), which absorb solar radiation extensively (Charabi and Bakhit, 2011). Moreover, vehicles, heat rejections from air conditions, factories and industries heat up urban areas rather than the surrounding environment. Lastly, high rise buildings reduce airflow and narrow lanes increase atmospheric temperature in compact urban areas, expanding the effect of heat island (Liu and Weng, 2012). Land surface temperature (LST) is an important indicator employed for assessing UHIs (Joshi and Bhatt, 2012). LST which is directly related to land surface characteristics is defined as radiometric temperature released from land surface and captured by a sensor at instant viewing angles (Zhou *et al.*, 2014, Zhou *et al.*, 2011). Land use pattern changes affect LST in urban environments (Singh *et al.*, 2017). Land uses have been changed by human requirements over time (Youneszadeh *et al.*, 2015). Therefore, there is an essential need to investigate spatio-temporal land use change and its effects on UHIs in order to find possible solution for them (Seif and Mokarram, 2012). Remote sensing (RS) is a beneficial tool for quantifying LST in response to land cover change (Orhan and Yakar, 2016). In other words, multi-temporal RS images could be applied to detect changes in surface cover and consequent changes in surface temperature (Seif and Mokarram, 2012; Butt *et al.*, 2015; Rajeshwari and Mani, 2014). Application of satellite images in obtaining LST dates back to 1970s (Carlson *et al.*, 1977). Since then, this topic has received extensive attentions internationally (Alavipanah *et al.*, 2015; Bai *et al.*, 2016; Kim and Ryu, 2015). For example, Gebeyehu Admasu (2017) employed the normalized difference vegetation index (NDVI), obtained from the Moderate Resolution Imaging Spectroradiometer (MODIS), to evaluate greenness and its link with LULC changes and rainfall in Addis Ababa over a 17-year period. The mentioned study revealed that the majority of Addis Ababa (86%) was converted to built-up area. Moreover, a considerable spatial reduction was found in the mean, maximum and standard deviations of NDVI, implying that the study area has become homogenous due to land conversions, particularly increased urbanization, at the expense of vegetation cover and agriculture. In another study, Ahmad (2012) conducted correlation analyses among four land cover indices (NDVI, normalized difference water index (NDWI), normalized difference built index (NDBI), and normalized difference bareness index (NDBaI)) and LST. The results demonstrated a positive correlation between surface temperature and NDBI and a negative correlation of surface temperature with NDVI, NDWI, and NDBaI. Ahmad (2012) concluded that the detected relationships are established by increase of built-up areas and decrease of vegetation and water covers. By the usage of RS/GIS for LULC change evaluation and assessing its effect on LST, Omran (2012) found that urban and barren lands have the highest LST, followed by waterlogged and vegetation. He also noted a negative correlation between NDVI and LST in all land use types. Kayet *et al.* (2016) considered the effects of ratio vegetation index (RVI) and soil adjusted vegetation index (SAVI) along with NDVI and NDBI on LST. The results of correlation analysis showed a negative relationship of LST with RVI, NDVI, and SAVI, and a positive relationship of LST with NDBI. Although UHIs in temperate regions have been extensively investigated, limited studies have been done on LST in arid urban areas (Lazzarini

et al., 2015). While temperate areas experience UHIs during daytime, arid urban areas are cooler than the surrounding contributing to the formation of urban cool islands (UCIs) (Cui and De Foy, 2012). Moreover, the impact of LULC changes on LST has not been well evaluated in most of arid areas which have been rapidly developed in recent years (Rasul *et al.*, 2017). For example, Al-Ali and Mubarak (2015) considered the effect of UHIs in Al Ahsa oasis in Saudi Arabia, ignoring higher LST in bare soils surrounding the city (which reverses UHI effects). Therefore, the present study aims to assess the effect of LULC changes on LST over time. Isfahan city in Iran, with a semi-arid climate, was selected as a study area due to its rapid growth and alterations in recent years. Change detection (examining LULC changes), LST changes assessment, and finding the relationships between LULC changes and LST are the main objectives pursued. This study has been conducted in Isfahan, Iran in 1985 and 2017.

MATERIALS AND METHODS

Study area

Isfahan is located in the central part of Iran at 32°39'8.86" N latitude and 51°40'28.63" E longitude (Fig. 1). This city, with an area of 15774 km^2 is the third largest city and one of the municipalities experiencing rapid development in Iran. Isfahan has a semi-arid climate, with an annual average temperature of 15.6 °C and an annual rainfall of 125 mm. July and January are the months with the highest (28.2°C) and the lowest (2.2°C) average temperatures in Isfahan, respectively. Looking for better livelihood, a large number of population have migrated from rural areas to Isfahan induced the replacement of natural and open lands by urbanized landscape (Climate-Data.Org, 2018). One of the main factors affecting Isfahan's climate is Zayandehrud River. Although the river was always flowing through Isfahan in last years, recently it has been dried out due to excessive water extraction at the upstream.

Data

Landsat satellite images have been widely used in local studies of LST (Li *et al.*, 2009, Amanollahi *et al.*, 2016). In this study, images from Landsat 5 Thematic Mapper (TM) for August 1985 and Landsat 8 Operational Land Imager (OLI) for August 2017 were applied for considering land use changes and their effect on LST. Cloud-free images (Raw = 37, Path = 164, Projection = UTM, Zone Number = 39N) were obtained from USGS Earth Resource Observation Systems Data Center, which had been gone through geometric and radiometric corrections (Sun *et al.*, 2010). Characteristics of selected images are provided in Table 1. Band 6 of TM and Band 10 of OLI were applied to retrieve LST. According to USGS instruction, it would be better not to use Band 11 of OLI in LST retrieval due to its larger calibration unreliability (Jeevalakshmi *et al.*, 2017). Near infrared (NIR) and Red bands were also applied to calculate NDVI.

Image classification for producing LULC map

LULC map of the study area was generated for 1985 and 2017 using the maximum likelihood supervised classification using Idrisi TerrSet. In supervised classification, firstly the number of land use classes is determined. Secondly, sample pixels (also known as training pixels), representing specific land use types, are selected by users. Training sites are then applied as references for classifying the entire image. In other words, training sites are used to calculate the mean and covariance of spectral bands for each land use class. The means and covariances are then applied

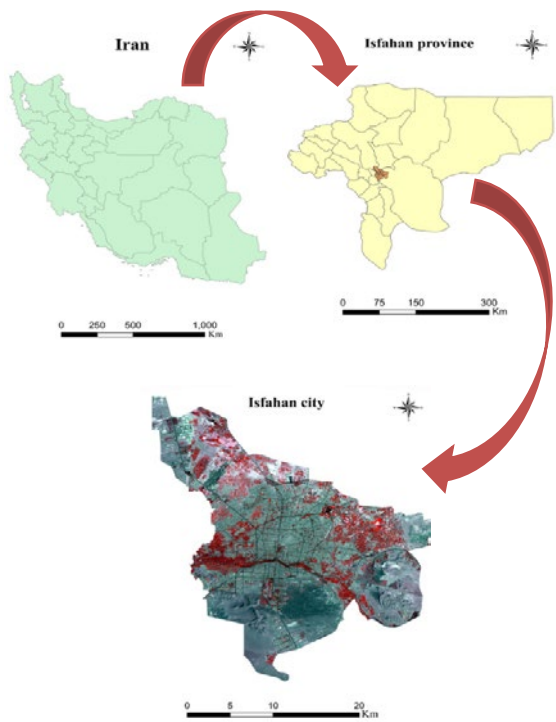

Fig. 1. Geographic location of the study area in Isfahan, Iran

Table 1. Characteristics of selected satellite images

Name	Date of capture	Number of bands	Bands wavelength (µm)
Landsat 5 Thematic Mapper (TM)	1985/08/02	7	Blue (0.45-0.52) Green (0.52-0.60) Red (0.63-0.69) Near Infrared (0.76-0.90) Shortwave Infrared 1 (1.55-1.75) Thermal (10.40-12.50) Shortwave Infrared 2 (2.08-2.35)
Landsat 8 Operational Land Imager (OLI)	2017/08/03	11	Coastal aerosol (0.43-0.45) Blue (0.45-0.51) Green (0.53-0.59) Red (0.64-0.67) Near Infrared (0.85-0.88) Shortwave Infrared 1 (1.57-1.65) Shortwave Infrared 2 (2.11-2.29) Panchromatic (0.50-0.68) Cirrus (1.36-1.34) Thermal Infrared 1 (10.60-11.19) Thermal Infrared 2 (11.50-12.51)

to allocate pixels into a particular land use (Briottet *et al.*, 2017, Ahmad and Quegan, 2012). Maximum likelihood is one of the algorithms applied to assign an unknown pixel to a specific land use type in supervised classification. The algorithm calculates the likelihood that a particular pixel is part of a specific land use type. Then the pixel is assigned to a land use with highest probability (Sisodia *et al.*, 2014). Four land use/cover classes were determined for the study area including built-up, vegetation, bare soil, and water. Selected Landsat images were segmented into regions associated with predetermined land use classes. In the next step, the representative sample segments of a specific cover type (training sites) were selected to drive spectral signature for each land use type. In the final step, maximum likelihood method was applied in supervised classification of the images, assigning equal probability values to each cover type.

Land surface temperature (LST)

LST is largely affected by land surface emissivity that is related to NDVI (Zhou *et al.*, 2014, Njoku, 2014). Therefore, NDVI-based emissivity method was applied in this study for extracting LST from Band 6 of Landsat TM 5 and Band 10 of Landsat 8 OLI, using the following process:

a) Calculation of top of the atmosphere (TOA) radiance: For TM 5 thermal band, the digital number (DN) of each pixel was converted to spectral radiance using Eq. 1 (NASA, 2010).

$$L_\lambda = \frac{L_{max\,\lambda} - L_{min\,\lambda}}{QCal_{max} - QCal_{min}} \times (QCal - QCal_{min}) + L_{min} \quad (1)$$

Where, L_λ is TOA spectral radiance (W/m^{2}sr µm); $L_{max\lambda}$ is spectral radiance scales to Q_{Calmax}; L_{min} is spectral radiance scales to Q_{Calmin}; Q_{Calmax} is the maximum quantized calibrated pixel value (typically=255); Q_{Calmin} is the minimum quantized calibrated pixel value (typically=1); and Q_{Cal} is quantized calibrated DN.

Equation 2 was employed to obtain TOA radiance for Landsat 8 OLI based on the radiance rescaling factors in Metadata file (Barsi *et al.*, 2014):

$$L_\lambda = M_L \times Q_{Cal} + A_L \quad (2)$$

Where, L_λ is TOA Spectral radiance (W/m^{2}sr µm), M_L is band-specific multiplicative rescaling factor; Q_{Cal} is quantized calibrated DN; and A_L is band-specific additive rescaling factors.

b) Calculation of brightness temperature (T_B): TOA radiance was transformed to brightness temperature with Eq. 3 (Giannini *et al.*, 2015).

$$T_B = \frac{K_2}{ln\left[\frac{K_1}{L_\lambda} + 1\right]} - 273.15 \quad (3)$$

Where, T_B is brightness temperature (K); L_λ is top of the atmosphere radiance ($W/m^2sr/\mu m$); K_1 and K_2 are calibration constants ($W/m^2sr\ \mu m$) which can be identified using the Metadata file associated with the satellite image; and -273.15 is used for converting brightness temperature from Kelvin to Celsius. c).

c) Calculation of NDVI: NDVI was calculated based on the reflectance values of visible red (ρ_{Red}) and near infrared (ρ_{NIR}) bands obtained by atmospheric correction according to Eq. 4 (Giannini *et al.*, 2015):

$$NDVI = \frac{\rho_{NIR}-\rho_{RED}}{\rho_{NIR}+\rho_{RED}} \quad (4)$$

Calculation of NDVI is necessary for calculating fractional vegetation cover (Pv) and emissivity (ε) in Steps d and e.;

d) Calculation of fractional vegetation cover (P_V): P_V value was calculated using $NDVI_{max}$ and $NDVI_{min}$, extracted in Step c as expressed by Eq. 5.

$$P_v = \left(\frac{NDVI - NDVI_{min}}{NDVI_{max} - NDVI_{min}}\right)^2 \quad (5)$$

e) Calculation of land surface emissivity (LSE or ε): An NDVI thresholds method was applied for LSE estimation from Landsat 8 OLI image using Eq. 6 (Jeevalakshmi *et al.*, 2017).

$$\varepsilon = \begin{cases} \varepsilon_w = 0.991 & \text{NDVI} \le 0 \\ \varepsilon_s = 0.966 & 0 < NDVI < 0.2 \\ \varepsilon_v P_v + \varepsilon_s(1 - P_v) + C_\lambda & 0.2 \le \text{NDVI} \le 0.5 \\ \varepsilon_v = 0.973 & \text{NDVI} > 0.5 \end{cases} \quad (6)$$

Where, ε_w, ε_v and ε_s are water, vegetation and soil emissivity, respectively, and C_λ is surface roughness considered as 0 for a flat surface. For calculating emissivity in Landsat TM 5, four cases were considered in Eq. 7 (Vlassova *et al.*, 2014).

$$\varepsilon = \begin{cases} \varepsilon_w = 0.985 & \text{NDVI} \le 0 \\ \varepsilon_s = 0.97 & 0 < NDVI < 0.2 \\ 0.004 \times P_v + 0.986 & 0.2 \le \text{NDVI} \le 0.5 \\ \varepsilon_v = 0.99 & \text{NDVI} > 0.5 \end{cases} \quad (7)$$

f) Calculation of LST: Eq. 8 was used to convert brightness temperature to land surface temperature (Orhan and Yakar, 2016):

$$LST = \frac{T_B}{1 + \left[\frac{\lambda * T_B}{\rho}\right] * ln(\varepsilon)} \quad (8)$$

Where, λ is emitted radiance wavelength (11.45 μm for Landsat TM 5 and 10.895μm for Landsat 8 OLI); ρ is equal to 0.01438 mK and is produced using ρ = h×c/b, in which "h" is the Planck's constant (6.626×10^{-34} Js), "c" is the velocity of light (2.998×108 m/s), and "b" is the Boltzmann constant (1.38×10^{-23} J/K); and ε is surface emissivity.

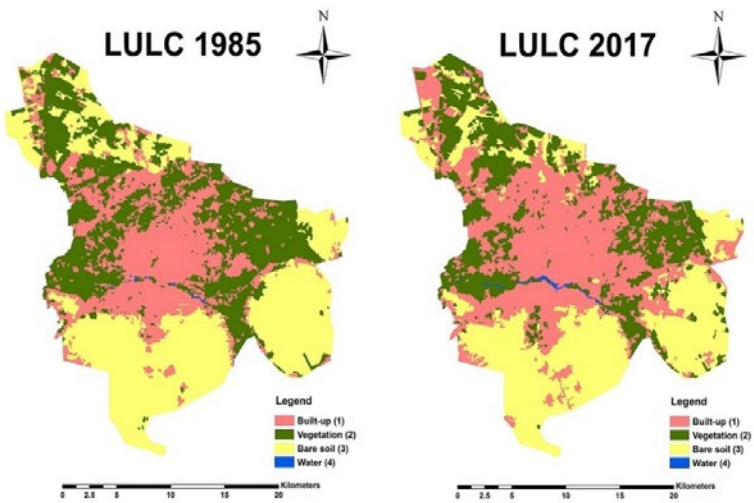

Fig. 2. Land use-Land cover maps of 1985 and 2017 in Isfahan

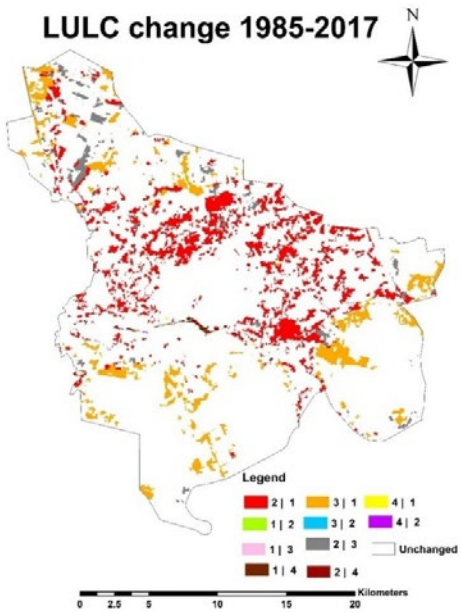

Fig. 3. LULC change from 1985 to 2017 in Isfahan

RESULTS AND DISCUSSION

Land-use/land-cover (LULC) changes during 1985 and 2017

LULC maps of Isfahan in 1985 and 2017 are illustrated in Fig. 2. Before change detection, it is essential to assess the accuracy of individual LULC classification (El-Hattab, 2016). 100 random check points were used to check the accuracy of the classified maps using Geographical Position System (GPS) and Google Earth for 2017 and aerial photographs and topographic maps for 1985. The most appropriate number of random check points for each class is "n(n + 1)" where n is the number of classes (El-Hattab, 2016). Error matrix was then created to compare reference data and classification results and to generate the overall accuracy and Kappa coefficient tables. The Kappa statistic considers the off-diagonal elements of the error matrix and represents the possibility of agreement between reference data and classification results occurring by chance (Bogoliubova and Tymków, 2014). Based on the results obtained from the error matrix, the overall accuracies of 1985 and 2017 images were 90% and 88% respectively. The Kappa coefficients for 1985 and 2017 were 85% and 82%, respectively. Considering different methods for land use classification including minimum distance of mean (MDM), Mahalanobis distance (MD), maximum likelihood (ML), artificial neural network (ANN), spectral angle mapper (SAM), and support vector machine (SVM), Yousefi *et al.* (2015) found ML and SVM as the most appropriate algorithms for preparing land use maps with Kappa of 0.94 and 0.93, respectively. In another study, Varamesh *et al.* (2017) generated land use maps based on object based image classification (OBIC) and maximum likelihood and found overall accuracy and kappa coefficients of 94.69% and 0.93 for OBIC and 81.53% and 0.75 for ML. They also concluded that accuracy rate over 85% is acceptable for land use mapping.

The classified images of both years show notable changes in the city in the last three decades. The post classification change detection technique (Alagu Raja *et al.*, 2013) was applied to monitor the size and distribution of land cover changes over the 32-year period (Table 2 and Fig. 3). To clarify Fig. 3 legend, Fig. 3 represents pattern of LULC change for 1985-2017 in which each land cover type is presented by a value (i.e. 1) built-up 2) vegetation 3) bare soil and 4) water. For example "2I1" in the legend indicates places where vegetation cover was converted to built-up areas from 1985-2017. As can be seen, built-up areas and water areas have been increased in 32 years. The share of built-up areas had an increase from 155.16 km^2 in 1985 to 216.71 km^2 in 2017, indicating conversion from vegetation cover and bare soil cover to built-up areas. Water

Table 2. Area of land-use/land-cover classes (1985 and 2017) in Isfahan

LULC Class	1985		2017		1985-2017	
	Area (km^2)	Total area (%)	Area (km^2)	Total area (%)	Change (km^2)	Change from original area (%)
Built-up	155.16	28.15	216.71	39.32	61.55	39.67
Vegetation	174.47	31.65	139.43	25.29	-35.04	-20.08
Bare soil	220.93	40.08	193.48	35.10	-27.45	-12.42
Water	0.635	0.12	1.58	0.29	0.945	148.82
Total	551.2		551.2		-	

bodies increased from 0.12% to 0.29%. In 1985, Zayandehrud River was dry as a result of no water discharge from the dam storing Zayandehrud water. However, in 2017 the river had flowed through Isfahan due to increase in water discharge. On the other hand, vegetation and bare soil covered larger areas in 1985 than in 2017. These decreasing trends might have two reasons. Vegetation and bare soil had been cleared to provide enough space for the increased population and required development. Due to unsuccessful agricultural practices/businesses and water shortage, some agricultural lands were abandoned by farmers, leading to reduction of vegetation cover and conversion to bare soil.

Changes in LSTs

Spatio-temporal distribution of LST in 1985 and 2017 is illustrated in Fig. 4 and Table 3. The estimated LST in August 1985 was in the range of 23.3°C to 47.4°C with an average value of 37.5°C and the variation of temperature in August 2017 was in the range of 22.8°C to 48.9°C with a mean value of 42.7°C. The highest average temperature was found in bare soil in both years. Higher temperature of bare soil compared to urban surfaces stems from higher solar radiation due to low reflectivity in barren lands (Georgescu *et al.*, 2011). Higher LST in urban areas compared to vegetation and water covers could be attributed to impenetrable surfaces including concretes, roads, and tiles extensively applied in urban areas (Zhang *et al.*, 2015). Moreover, higher soil moisture in urban areas in contrast to bare soil resulted in evaporation from soil and thereby reduced LST (Rasul *et al.*, 2016). Notably, there is a major distinction between the findings of previous studies and the results obtained in the current study. Previous studies indicated a higher temperature in urban areas than in surrounding areas (mostly vegetation), leading to formation of UHIs. However, this study revealed that the built up areas experienced a cooler LST compared to the surroundings areas (mostly covered by bare lands). This conflict can be due to various climatic conditions in the selected study area and tropical, Mediterranean and cold cities

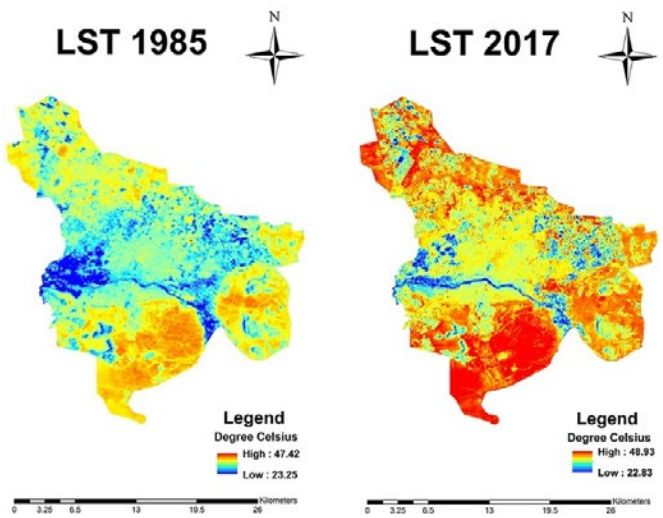

Fig. 4. LST maps in 1985 and 2017 in Isfahan

Table 3. Land surface temperature distribution over LULC classes between 1985 and 2017 in Isfahan

LULC	LST (°C), August 1985			LST (°C), August 2017			LST between 1985-2017
	Min	Max	Average	Min	Max	Average	
Built-up	24.54	44.86	36.93	23.40	48.93	42.45	5.52
Vegetatio	23.25	43.35	34.13	25.08	48.93	38.87	4.74
Bare soil	26.68	47.42	40.66	27.83	48.93	45.88	5.22
Water	24.97	38.01	31.09	22.83	42.49	29.48	-1.61

considered in previous studies. In the semi-arid climate of the study area, urban green areas may reduce LST through evaporative cooling. Therefore, urban centers experience a lower temperature than the surroundings with a low soil water content, sparse vegetation, and bare sandy soil. There are limited evidences that arid urban areas exhibit UHIs during nights and UCIs during daytime (Clinton and Gong, 2013, Keramitsoglou *et al.*, 2011). Further studies are recommended to obtain a comprehensive view on LULC changes effects on LST in semi-arid areas using nocturnal satellite images. On the other hand, water and vegetation covers had the lowest average LST both in 1985 and 2017. High thermal capacity in water leads to low surface temperature in water bodies compared to other land use types (Dong *et al.*, 2018). Increase of water content in Zayandehrud resulted in cool temperature in some parts of the city in 2017 compared to 1985. Cooling role of water is also emphasized in the related literature (Deng *et al.*, 2018, Xiao *et al.*, 2018). Lower temperature of vegetation compared to built-up and bare soil is due to transpiration in dense vegetation which reduces the amount of heat store in the surface (Pal and Ziaul, 2017).

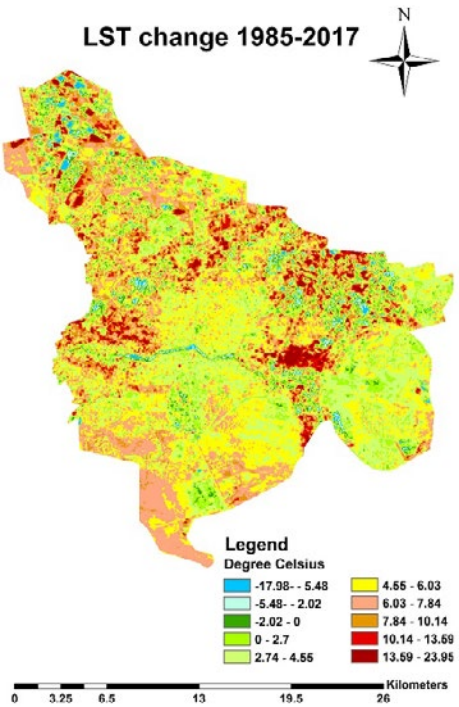

Fig. 5. LST changes from 1985 to 2017 in Isfahan

Comparison of retrieved LSTs in this study with the temperature of a ground monitoring station revealed that ground station temperature data did not match with LST obtained using satellite data. There is only one station in Isfahan for recording temperature which cannot provide detailed information on LST variations in all areas of the city. In other words, satellite images provide information on temperature dispensation over large scales which cannot be covered using a single ground station data. Numerous studies have reported both similarities (Mutiibwa *et al.*, 2015) and dissimilarities (Amanollahi *et al.*, 2016) between LST and air temperature measured in ground station. However, this contrast has not been fully understood yet (Tomlinson *et al.*, 2011).

Land-use/land-cover changes and land surface temperature relations

The effect of LULC conversion on LST is summarized in Fig. 5 and Table 4. As illustrated, the locations representing high LST were in fact the areas where vegetation was converted to bare soil (9.16 °C) and urban areas (8.41 °C). A marked city development took place in northern bank of Zayandehrud. In this area, vegetation covers were mostly replaced by built-up areas resulted in LST increase between 1985 and 2017. Vegetation removal increases carbon dioxide accumulation in the atmosphere that in turn affects global surface energy budget (Islam and Islam, 2013). Moreover, the growth of settlement increased LST by converting the vegetation to non-evaporating surface. Overall, the results confirmed the decreasing effect of vegetation and increasing effect of built-up

Table 4.LST (°C) with respect to LULC changes

LULC changes	Average LST August 1985	Average LST August 2017	Average change in LST 1985-2017
Vegetation to built-up	34.41	42.82	8.41
Bare soil to built-up	40.52	44.59	4.07
Vegetation to bare soil	37.21	46.37	9.16
Vegetation to water	29.10	28.46	-0.64

areas on LST variations, which is also emphasized in other studies (Singh *et al.*, 2017, Amanollahi *et al.*, 2016). In addition to land cover changes, population of urban areas contribute to increase of LST by rising the anthropogenic heat discharge (Zhou and Wang, 2011). The results also implied that increase of LST in the bare soil converted to built-up might be related to global warming. The temperature of urban land increased by the increase of CO_2 in upper atmosphere of the Earth. LST increase in the lands converted from bare soils to built-up areas might have another reason. Since the converted urban areas with built-up covers are fragmented in barren lands, they can be influenced by the temperature distribution from bare soil, which increases the temperature of fragmented built-up covers. Decrease of LST was found where vegetation covers had been converted to water, which is expected due to lower surface temperature of water compared to other land use types. However, this type of conversion had occurred in limited places.

CONCLUSION

Various land covers with different solar reflectivity (albedo), thermal conductivity, surface roughness and heat capacity experience different LST. Assessment of land cover impact on LST through RS data has received considerable attentions from researchers in recent years. Moreover, this topic is an area of concern for environmental scientists and planners due to the effect of urban temperature on population health. In the current study, it was tried to quantify variations in land use and consequently in land surface temperature over three decades in Isfahan, one of the fast-growing cities in Iran with semi-arid climate. The results obtained by application of thermal RS data and GIS techniques revealed that LULC and consequently LST had experienced extensive alterations in a 32-year period. According to the result build up areas, vegetation covers and bare soil exhibited 5.52°C, 4.72°C, and 5.22°C rise in surface temperature from 1985 to 2017. On the other hand, water bodies experienced -1.61°C reduction in surface temperature in 2017 compared to 1985. It was also found that LST variation in the study area was related to the LULC changes. While the transformation of vegetation and bare soil to build-up areas increased surface temperature by 8.41°C and 4.07°C, vegetation transformation to bare soil and water resulted in 9.16°C increase and -0.64°C decrease in surface temperature. Unlike tropical, Mediterranean and cold cities which experience the urban heat island effect, Isfahan, with its semi-arid climate, experienced the urban cool island effect. Cool islands in Isfahan are produced by the surrounding bare soils with high surface temperature enclosing the built-up areas. Increase in temperature could cause issues in energy demand, water demand, infrastructure, and health. The results obtained in this study can be applied by decision makers as an environmental assessment tool for urban development. In other words, LST and LULC change information may be applied to construct an appropriate thermal environment through land use management. To have more detailed view on land surface temperature in urban areas, it is suggested to: 1) Conduct the same investigation at night to evaluate nocturnal LST variations in arid areas; 2) Apply other algorithms including single-channel, split-window and multi-angle techniques for extracting more accurate LST maps.

ACKNOWLEDGEMENTS

The authors would like to thank Vice Chancellor for Research, University of Kurdistan for providing research Grant number [97/11/270] to conduct this study.

CONFLICT OF INTERESTS

The author declares that there is no conflict of interests regarding the publication of this manuscript. In addition, the ethical issues, including plagiarism, informed consent, misconduct, data fabrication and/or falsification, double publication and/or submission, and redundancy have been completely observed by the authors.

ABBREVIATIONS

ε	Emissivity
ε_s	Soil emissivity
ε_v	Vegetation emissivity
ε_w	Water emissivity
λ	Emitted radiance wavelength
ρ_{NIR}	Reflectance values of near infrared
ρ_{Red}	Reflectance values of visible red
A_L	Band-specific additive rescaling factors
ANN	Artificial neural network
b	Boltzmann constant

c	Velocity of light
^{O}C	Celsius degree
DN	Digital number
GPS=	Geographical Position System
h	Planck's constant
IPCC	Intergovernmental Panel on Climate Change
K_1 *and* K_2	Calibration constants
L_λ	TOA spectral radiance
$L_{max\lambda}$	Spectral radiance scales to Q_{Calmax}
$L_{min\lambda}$	Spectral radiance scales to Q_{Calmin}
LSE	Land surface emissivity
LST	Land surface temperature
LULC	Land-use/land-cover
MD	Mahalanobis distance
MDM	Minimum distance of mean
M_L	Band-specific multiplicative rescaling factor
ML	Maximum likelihood
MODIS	Moderate resolution imaging spectroradiometer
n	Number of classes
NDBaI	Normalized difference bareness index
NDBI	Normalized difference built
NDVI	Normalized difference vegetation index
NDWI	Normalized difference water index
OBIC	Object based image classification
OLI	Operational land imager
Pv	Fractional vegetation cover
Q_{Cal}	Quantized calibrated DN
Q_{Calmax}	The maximum quantized calibrated pixel value
Q_{Calmin}	The minimum quantized calibrated pixel value
RS	Remote sensing
RVI	Ratio vegetation index
SAM	Spectral angle mapper
SAVI	Soil adjusted vegetation index
SVM	support vector machine
T_B	Brightness temperature
TM	Thematic Mapper
TOA	Top of the atmosphere
UCIs	Urban cool islands
UHIs	Urban heat islands

REFERENCES

Ahmad, F., (2012). Detection of change in vegetation cover using multi-spectral and multi-temporal information for District Sargodha, Pakistan. Soc. Nat., 24(3): 557-571 **(15 pages).**

Ahmad, A.; Quegan, S., (2012). Analysis of maximum likelihood classification on multispectral data. Appl. Math. Sci., 6(129): 6425-6436 **(12 pages).**

Al-Ali, A.; Mubarak, H., (2015). The effect of land cover on the air and surface urban heat island of a desert Oasis. PhD, Durham University.

Alagu Raja, R.A.; Anand, V.; Senthil Kumar, A.; Sandeep Maithani, V.; Kumar, A., (2013). Wavelet based post classification change detection technique for urban growth monitoring. J. Indian Soc. Remote Sens., 41: 35-43 **(9 pages).**

Alavipanah, S.; Wegmann, M.; Qureshi, S.; Weng, Q.; Koellner, T., (2015). The role of vegetation in mitigating urban land surface temperatures: A case study of Munich, Germany during the warm season. Sustainability, 7(4): 4689-4706 **(18 pages)**.

Amanollahi, J.; Tzanis, C.; Ramli, M. F.; Abdullah, A. M., (2016). Urban heat evolution in a tropical area utilizing Landsat imagery. Atmos. Res., 167: 175-182 **(8 pages)**.

Bai, L.; Woodward, A.; Liu, Q., (2016). County-level heat vulnerability of urban and rural residents in Tibet, China. J. Environ. Health., 15(1): 3-13 **(11 pages)**.

Barsi, J. A.; Schott, J. R.; Hook, S. J.; Raqueno, N. G.; Markham, B. L.; Radocinski, R. G., (2014). Landsat-8 thermal infrared sensor (TIRS) vicarious radiometric calibration. Remote Sens., 6(11): 11607-11626 **(20 pages)**.

Bogoliubova, A.; Tymków, P., (2014). Accuracy assessment of automatic image processing for land cover classification of ST.Petersburg protected area. Geodesia et Descriptio Terrarum, 13(1-2): 5-22 **(18 pages)**.

Briottet, X.; Chehata, N.; Oltra-Carrio, R.; Le Bris, A.; Weber, C., (2017). Optical remote sensing in urban environment, in: Baghdadi, N., Zribi, M. (Eds.), Land Surf. Remote Sens. Urban Coast. Areas. Elsevier. 1- 62 **(62 pages).**

Butt, A.; Shabbir, R.; Ahmad, S. S.; Aziz, N., (2015). Land use change mapping and analysis using remote sensing and GIS: A case study of Simly watershed, Islamabad, Pakistan. Egypt. J. Remote Sens. Space Sci., 18(2): 251-259 **(9 pages)**.

Carlson, T.; Augustine, J.; Boland, F., (1977). Potential application of satellite temperature measurements in the analysis of land use over urban areas. Bull. Am. Meteorol. Soc., 1301-1303 **(3 pages)**.

Charabi, Y.; Bakhit, A., (2011). Assessment of the canopy urban heat island of a coastal arid tropical city: The case of Muscat, Oman. Atmos. Res., 101(1-2): 215-227 **(13 pages)**.

Chen, F.; Yang, X.; Zhu, W., (2014). WRF simulations of urban heat island under hot-weather synoptic conditions: The case study of Hangzhou City, China. Atmos. Res., 138: 364-377 **(14 pages)**.

Clinton, N.; Gong, P., (2013). MODIS detected surface urban heat islands and sinks: Global locations and controls. Remote Sens. Environ., 134: 294-304 **(11 pages)**.

Cui, Y. Y.; De Foy, B., (2012). Seasonal variations of the urban heat island at the surface and the near-surface and reductions due to urban vegetation in Mexico City. J. Appl. Meteorol. Climatol.,

51(5): 855-868 **(14 pages)**.

Deng, Y.; Wang, S.; Bai, X.; Tian, Y.; Wu, L.; Xiao, J.; Chen, F.; Qian, Q., (2018). Relationship among land surface temperature and LUCC, NDVI in typical karst area. Sci. Rep., 8(1): 641-653 **(13 pages)**.

Dong, F.; Chen, J.; Yang, F., (2018). A Study of Land Surface Temperature Retrieval and Thermal Environment Distribution Based on Landsat-8 in Jinan City. Conf. Ser.: Earth Environ. Sci., 118 **(11 pages)**.

El-Hattab, M. M., (2016). Applying post classification change detection technique to monitor an Egyptian coastal zone (Abu Qir Bay). Egypt. J. Remote Sens. Space Sci., 19(1): 23-36 **(14 pages)**.

Gebeyehu Admasu, T., (2017). Monitoring trends of greenness and LULC (land use/land cover) change in Addis Ababa and its surrounding using MODIS time-series and LANDSAT Data. Master of Science, Lund University. Sweden.

Georgescu, M.; Moustaoui, M.; Mahalov, A.; Dudhia, J., (2011). An alternative explanation of the semiarid urban area "Oasis Effect". J. Geophys. Res. D: Atmos., 116(D24). **(13 pages).**

Giannini, M.; Belfiore, O.; Parente, C.; Santamaria, R., (2015). Land Surface Temperature from Landsat 5 TM images: comparison of different methods using airborne thermal data. J. Eng. Sci. Technol. Rev., 8(3): 83-90 **(8 pages)**.

Howard, L., (1818). The climate of London: Deduced from Meteorological Observations. Cambridge.

Islam, M. S.; Islam, K. S., (2013). Application of thermal infrared remote sensing to explore the relationship between land use-land cover changes and urban heat Island effect: a case study of Khulna City. Journal of BIP, 6: 49-60 **(12 pages)**.

Jeevalakshmi, D.; Reddy, S.; Manikiam, B., (2017). Land Surface Temperature Retrieval from LANDSAT data using Emissivity Estimation. Int. J. Appl. Eng. Res, 12(20): 9679-9687 **(9 pages)**.

Joshi, J. P.; Bhatt, B., (2012). Estimating temporal land surface temperature using remote sensing: A study of Vadodara urban area, Gujarat. JGEE, 2(1): 123-130 **(8 pages)**.

Kayet, N.; Pathak, K.; Chakrabarty, A.; Sahoo, S., (2016). Urban heat island explored by co-relationship between land surface temperature vs multiple vegetation indices. Spat. Inf. Res., 24(5): 515-529 **(15 pages)**.

Keramitsoglou, I.; Kiranoudis, C. T.; Ceriola, G.; Weng, Q.; Rajasekar, U., (2011). Identification and analysis of urban surface temperature patterns in Greater Athens, Greece, using MODIS imagery. Remote Sens. Environ., 115(12): 3080-3090 **(11 pages)**.

Kim, S.; Ryu, Y., (2015). Describing the spatial patterns of heat vulnerability from urban design perspectives. Int J Sust Dev World., 22(3): 189-200 **(12 pages)**.

Lazzarini, M.; Molini, A.; Marpu, P. R.; Ouarda, T. B.; Ghedira, H., (2015). Urban climate modifications in hot desert cities: The role of land cover, local climate, and seasonality. Geophys. Res. Lett., 42(22): 9980-9989 **(10 pages)**.

Li, J.; Wang, X.; Wang, X.;Ma, W.; Zhang, H., (2009). Remote sensing evaluation of urban heat island and its spatial pattern of the Shanghai metropolitan area, China. Ecol. Complexity, 6(4): 413-420 **(8 pages)**.

Liu, H.; Weng, Q., (2012). Enhancing temporal resolution of satellite imagery for public health studies: A case study of West Nile Virus outbreak in Los Angeles in 2007. Remote Sens. Environ., 117: 57-71 **(15 pages)**.

Mutiibwa, D.; Strachan, S.; Albright, T., (2015). Land surface temperature and surface air temperature in complex terrain. IEEE J. Sel. Top. Appl. Earth Obs. Remote Sens., 8(10): 4762-4774 **(13 pages)**.

NASA., (2010). Landsat 7 Science Data User Handbook: National Aeronautics and Space Administration.

Njoku, E.G., (2014). Encyclopedia of Remote Sensing., Berlin. Germany. Ed. Springer.

Omran, E., (2012). Detection of land-use and surface temperature change at different resolutions. J. Geogr. Inf. Syst., 4(03): 189-203 **(15 pages).**

Orhan, O.; Yakar, M., (2016). Investigating Land Surface Temperature Changes Using Landsat Data in Konya, Turkey. ISPRS Archives, 41 (B8): 12-19 **(8 pages)**.

Pal, S.; Ziaul, S., (2017). Detection of land use and land cover change and land surface temperature in English Bazar urban center. Egypt. J. Remote Sens. Space Sci., 20(1): 125-145 **(21 pages)**.

Rajeshwari, A.; Mani, N., (2014). Estimation of land surface temperature of Dindigul district using Landsat 8 data. IJRET, 3(5): 122-126 **(5 pages)**.

Rasul, A.; Balzter, H.; Smith, C., (2016). Diurnal and seasonal variation of surface urban cool and heat islands in the semi-arid city of Erbil, Iraq. Climate, 4(3): 42-58 **(17 pages)**.

Rasul, A.; Balzter, H.; Smith, C.; Remedios, J.; Adamu, B.; Sobrino, J. A.; Srivanit, M.; Weng, Q., (2017). A review on remote sensing of urban heat and cool islands. Land, 6(2): 38.

Seif, A.; Mokarram, M., (2012). Change detection of Gil Playa in the Northeast of Fars Province. Iran Am. J. Sci. Res, 86: 122-130 **(9 pages)**.

Singh, P.; Kikon, N.; Verma, P., (2017). Impact of land use change and urbanization on urban heat island in Lucknow city, Central India. A remote sensing based estimate. Sustain Cities Soc., 32: 100-114 **(15 pages)**.

Sisodia, P. S.; Tiwari, V.; Kumar, A., (2014). Analysis of supervised maximum likelihood classification for remote sensing image. In Recent Advances and Innovations in Engineering (ICRAIE). Jaipur, India.

Sun, Q.; Tan, J.; Xu, Y., (2010). An ERDAS image processing method for retrieving LST and describing urban heat evolution: a case study in the Pearl River Delta Region in South China. Environ. Earth Sci., 59(5): 1047-1055 **(9 pages)**.

Tomlinson, C. J.; Chapman, L.; Thornes, J. E.; Baker, C., (2011). Remote sensing land surface temperature for meteorology and climatology: A review. Meteorol. Appl., 18(3): 296-306 **(11 pages)**.

Varamesh, S.; Hosseini, S.M.; Rahimzadegan, M., (2017). Comparison of conventional and advanced classification approaches by Landsat-8 imagery. App.l Ecol. Environ. Res., 15(3): 1407-1416 **(10 pages).**

Vlassova, L.; Perez-Cabello, F.; Nieto, H.; Martín, P.; Riaño, D.; de la Riva, J., (2014). Assessment of methods for land surface

temperature retrieval from Landsat-5 TM images applicable to multiscale tree-grass ecosystem modeling. Remote Sens., 6(5): 4345-4368 **(24 pages)**.

Xiao, H.; Kopecká, M.; Guo, S.; Guan, Y.; Cai, D.; Zhang, C.; Zhang, X.; Yao, W., (2018). Responses of Urban Land Surface Temperature on Land Cover: A Comparative Study of Vienna and Madrid. Sustainability, 10(2): 1-19 **(19 pages)**.

Yıldırım, Ü.; Erdoğan, S.; Uysal, M., (2011). Changes in the coastline and water level of the Akşehir and Eber Lakes between 1975 and 2009. Water Resour. Manage., 25(3): 941-962 **(22 pages)**.

Youneszadeh, S.; Amiri, N.; Pilesjo, P., (2015). The effect of land use change on land surface temperature in the Netherlands. Int. Arch. Photogramm. Remote Sens. Spatial Inf. Sci., XL-1/W5: 745-748 **(4 pages)**.

Yousefi, S.; Mirzaee, S.; Tazeh, M; Pourghasemi, H.; Karimi, H., (2015). Comparison of different algorithms for land use mapping in dry climate using satellite images: a case study of the Central regions of Iran. Desert., 20 (1): 1-10 **(10 pages).**

Zhang, Y.; Balzter, H.; Zou, C.; Xu, H.;Tang, F., (2015). Characterizing bi-temporal patterns of land surface temperature using landscape metrics based on sub-pixel classifications from Landsat TM/ETM+. Int. J. Appl. Earth Obs. Geoinf., 42: 87-96 **(10 pages)**.

Zhou, W.; Huang, G.; Cadenasso, M. L., (2011). Does spatial configuration matter? Understanding the effects of land cover pattern on land surface temperature in urban landscapes. Landscape Urban Plann., 102(1): 54-63 **(10 pages)**.

Zhou, W.; Qian, Y.; Li, X.; Li, W.; Han, L., (2014). Relationships between land cover and the surface urban heat island: seasonal variability and effects of spatial and thematic resolution of land cover data on predicting land surface temperatures. Landscape Ecol., 29(1): 153-167 **(15 pages)**.

Zhou, X.; Wang, Y., (2011). Dynamics of Land Surface Temperature in Response to Land-Use/Cover Change. Geographical Research, 49(1): 23-36 **(14 pages)**.

AUTHOR (S) BIOSKETCHES

Reisi, M., Ph.D., Assistant Professor, Department of Environmental Sciences, Faculty of Natural Resources, University of Kurdistan, Sanandaj, Iran. Email: *bryanallan.talisay@gmail.com*

Ahmadi Nadoushan, M., Ph.D., Assistant Professor, Department of Environmental Sciences, Isfahan (Khorasgan) Branch, Islamic Azad University, Isfahan, Iran. Email: *m.ahmadi@khuisf.ac.ir*

Aye, L., Ph.D., Professor, Renewable Energy and Energy Efficiency Group, Department of Infrastructure Engineering, Melbourne School of Engineering, The University of Melbourne, VIC 3010, Australia. Email: *l.aye@unimelb.edu.au*

COPYRIGHTS

Copyright for this article is retained by the author(s), with publication rights granted to the GJESM Journal. This is an open-access article distributed under the terms and conditions of the Creative Commons Attribution License (http://creativecommons.org/licenses/by/4.0/).

HOW TO CITE THIS ARTICLE

Reisi, M.; Ahmadi Nadoushan, M.; Aye, L., (2019). Land surface temperature responses to land use-cover change in semi-arid urban areas. Global J. Environ. Sci. Manage., 5(3): 319-330.

DOI: 10.22034/gjesm.2019.03.05

url: https://www.gjesm.net/article_35131.html